Monthly Notices
of the
ROYAL ASTRONOMICAL SOCIETY

MNRAS **463,** 3193–3203 (2016)
Advance Access publication 2016 September 7

doi:10.1093/mnras/stw2198

Observational challenges in Lyα intensity mapping

P. Comaschi,[1]★ B. Yue[1] and A. Ferrara[1,2]

[1]*Scuola Normale Superiore, Piazza dei Cavalieri 7, I-1-56126 Pisa, Italy*
[2]*Kavli IPMU, The University of Tokyo, 5-1-5 Kashiwanoha, Kashiwa 277-8583, Japan*

Accepted 2016 August 27. Received 2016 August 27; in original form 2016 May 18

ABSTRACT

Intensity mapping (IM) is sensitive to the cumulative line emission of galaxies. As such, it represents a promising technique for statistical studies of galaxies fainter than the limiting magnitude of traditional galaxy surveys. The strong hydrogen Lyα line is the primary target for such an experiment, as its intensity is linked to star formation activity and the physical state of the interstellar and intergalactic medium. However, to extract the meaningful information, one has to solve the confusion problems caused by interloping lines from foreground galaxies. We discuss here the challenges for a Lyα IM experiment targeting $z > 4$ sources. We find that the Lyα power spectrum can be, in principle, easily (marginally) obtained with a 40 cm space telescope in a few days of observing time up to $z \lesssim 8$ ($z \sim 10$) assuming that the interloping lines (e.g. Hα, [O II], [O III] lines) can be efficiently removed. We show that interlopers can be removed by using an ancillary photometric galaxy survey with limiting AB mag ∼26 in the near-infrared bands (Y, J, H, or K). This would enable detection of the Lyα signal from $5 < z < 9$ faint sources. However, if a [C II] IM experiment is feasible, by cross-correlating the Lyα with the [C II] signal, the required depth of the galaxy survey can be decreased to AB mag ∼24. This would bring the detection at the reach of future facilities working in close synergy.

Key words: cosmic background radiation – cosmology: observations – diffuse radiation – large-scale structure of Universe – infrared: diffuse background.

1 INTRODUCTION

One of the key open problems in cosmology is the origin and evolution of galaxies and their stars. In the last decade, astonishing technological progresses have allowed us to probe galaxies located within less than one billion year from the big bang (Ouchi et al. 2008, 2010; Bouwens et al. 2014a; Oesch et al. 2014, 2015; Matthee et al. 2015). These searches reveal an early Universe in which complex phenomena were simultaneously taking place, ranging from the formation of supermassive black holes (Volonteri & Bellovary 2012) to the reionization process, (Barkana & Loeb 2001), along with the metal enrichment by the first stars (Ferrara 2016).

High-redshift sources are very faint and their detection is remarkably challenging: up to now, less than 1000 galaxies have been detected at $z \gtrsim 8$, and among them only a handful are at $z \sim 10$ (e.g. Bouwens et al. 2014b; Calvi et al. 2016; McLeod, McLure & Dunlop 2016). Moreover, it is believed that low-mass galaxies have a dominant role (Salvaterra, Ferrara & Dayal 2011) in driving reionization, while the most luminous ones appear to be only rare outliers. Such ultrafaint galaxies are likely to remain undetected even by the next generation observatories, such as JWST,[1] TMT[2] or E-ELT.[3]

A novel approach has been proposed to overcome the problem and study, at least statistically, the early faint galaxy population. Basically, the idea is to trade the ability to resolve individual sources, with a statistical analysis of the cumulative signal produced by the entire population (Kashlinsky 2005; Cooray 2016). Intensity mapping (IM; see e.g. Visbal & Loeb 2010; Visbal, Trac & Loeb 2011) is one implementation of such a concept and aims at detecting 3D large-scale emission line fluctuations. In the last years, this concept has become very popular and several lines have been proposed as candidates. Among these are the H I 21cm (Furlanetto, Oh & Briggs 2006), CO (Righi, Hernández-Monteagudo & Sunyaev 2008; Lidz et al. 2011; Breysse, Kovetz & Kamionkowski 2014), C II (Gong et al. 2012; Silva et al. 2015; Yue et al. 2015), H_2 (Gong, Cooray & Santos 2013), He II (Visbal, Haiman & Bryan 2015) and Lyα (Silva et al. 2013; Pullen, Doré & Bock 2014; Comaschi & Ferrara 2016) emission lines.

Although IM experiments seem indeed promising, their reliability has not yet been convincingly demonstrated. In particular,

★E-mail: paolo.comaschi@sns.it

[1] http://www.jwst.nasa.gov
[2] http://www.tmt.org
[3] https://www.eso.org/sci/facilities/eelt/

continuum foregrounds dominate over line intensity by several orders of magnitude: cleaning algorithms have been developed for 21 cm radiation (Wang et al. 2006; Chapman et al. 2015; Wolz et al. 2015), but are not comparably well understood for other lines (Yue et al. 2015). Moreover, some lines (such as Lyα and FIR emission lines) suffer from line confusion: for example, the Hα line ($\lambda_{\mathrm{H}\alpha} = 0.6563\,\mu$m), if emitted at $z = 0.48$, can be misclassified as a Lyα line emitted at $z = 7$ (Gong et al. 2014). We will refer to such intervening sources as interlopers.

Considering that the first generation of instruments devoted to IM are starting to be proposed or funded (Crites et al. 2014; Doré et al. 2014; Cooray et al. 2016), it is essential to gain a deeper understanding of the difficulties implied by an IM experiment. This forms the motivation of this work and we will pay particular attention to the Lyα emission line which is the most luminous UV line and one of the most promising candidates for an IM survey in the near-infrared (NIR) spectral region.

Lyα emission is associated with UV and ionizing radiation and therefore is strongly correlated with the star formation rate (SFR) in galaxies. Moreover, the reprocessing of UV photons by neutral hydrogen in the intergalactic medium (IGM) also produces Lyα photons. Some recent works have predicted the power spectrum (PS) of the target line and assessed its observability. Pullen et al. (2014) and Silva et al. (2013) developed analytical models for the Lyα PS and showed that it is at the reach of a small space instrument. Gong et al. (2014) used the model developed by Silva et al. (2013) to study the problem of line confusion, finding that masking bright voxels can represent a viable strategy. In a similar attempt, Breysse, Kovetz & Kamionkowski (2015) pointed out that masking bright voxels is an effective strategy for the removal of the interlopers, but it might jeopardize the recovered line PS, causing loss of astrophysical information.

A realistic Lyα model has to deal with all the astrophysics processes (e.g. star formation, radiative transfer) self-consistently. This is rather challenging even for high-resolution hydrodynamic simulations. Alternatively, a viable strategy for studying such complex processes is to develop an analytical model that includes all the theoretical uncertainties represented by a few parameters: in this way, it is possible to understand easily how the results depends on the unknowns and what is the available parameter space of the problem yielding solution compatible with existing observations. Comaschi & Ferrara (2016) (hereafter CF16) developed an analytical model for diffuse Lyα intensity and its PS, with a focus on IM at the epoch of reionization (EoR). The model is observation-driven and it includes the most recent determinations both for galaxies and IGM. They associated dust-corrected UV luminosity to dark matter haloes by the abundance matching technique (Vale & Ostriker 2004; Conroy & Wechsler 2009; Behroozi, Conroy & Wechsler 2010), using the Luminosity Function (LF) from the *Hubble* legacy fields (Bouwens et al. 2015), and the UV luminosity spectral slope in Bouwens et al. (2014a). Then using a template spectral energy distribution from STARBURST99[4] (Leitherer et al. 1999; Vázquez & Leitherer 2005; Leitherer et al. 2014) and the Calzetti extinction law (Calzetti et al. 2000), they were able to model self-consistently the interaction of ionizing photons with the interstellar medium (ISM) and the IGM, calibrating the poorly constrained parameters in order to have a realistic reionization history (Fan et al. 2006; Planck Collaboration XIII 2015).

[4] http://www.stsci.edu/science/starburst99/docs/default.htm

CF16 found that for Lyα, absolute intensity is dominated by recombinations in ISM ($\nu I_\nu^{\mathrm{ISM}}(z = 4[7]) = 7.81[1.18] \times 10^{-2}\,\mathrm{nW\,m^{-2}\,sr^{-1}}$), and Lyman continuum absorption and relaxation in the IGM ($\nu I_\nu^{\mathrm{IGM}}(z = 4[7]) = 10.3[2.39] \times 10^{-2}\,\mathrm{nW\,m^{-2}\,sr^{-1}}$), with the latter being about a factor of 1.3(2) stronger at $z = 4(7)$. However, intensity fluctuations are mostly contributed by the ISM emission on all scales $<100\,h^{-1}$ Mpc. Such scale essentially corresponds to the distance at which UV photons emitted by galaxies are redshifted into Lyα resonance.

The comoving Lyα luminosity density from IGM and galaxies is $\dot{\rho}_{\mathrm{Ly}\,\alpha}^{\mathrm{IGM}}(z = 4[7]) = 8.73[6.51] \times 10^{40}\,\mathrm{erg\,s^{-1}\,Mpc^{-3}}$ and $\dot{\rho}_{\mathrm{Ly}\,\alpha}^{\mathrm{ISM}}(z = 4[7]) = 6.62[3.21] \times 10^{40}\,\mathrm{erg\,s^{-1}\,Mpc^{-3}}$. Remarkably, CF16 is consistent with recent Sloan Digital Sky Survey (SDSS) observations at $z \approx 2.5$ if extrapolated to lower redshift (Croft et al. 2015, $\dot{\rho}_{\mathrm{Ly}\,\alpha}^{\mathrm{SDSS}} \approx 3 \times 10^{41}\,\mathrm{erg\,s^{-1}\,Mpc^{-3}}$). CF16 predicts a power $k^3 P^{\mathrm{Ly}\,\alpha}(k, z)/2\pi^2 = 9.76 \times 10^{-4}(2.09 \times 10^{-5})\mathrm{nW^2\,m^{-4}\,sr^{-2}}$ at $z = 4(7)$ for $k = 0.1\,h\,\mathrm{Mpc^{-1}}$.

We present in the following a feasibility study of a Lyα IM survey based on CF16 results. In particular, we tackle the problem of (i) required sensitivity; (ii) suppression of line confusion through interlopers removal; (iii) detectability of the cross-correlation with the C II line. The paper is organized as follows: in Section 2, we compute in a general way the signal-to-noise ratio (S/N) of an IM observation; in Section 3, we model the sensitivity of an intensity mapper and compute the S/N of an observation; in Section 4, we analyse the problem of line confusion. Section 5 contains a study of the cross-correlation between Lyα and C II emission and of the S/N of a realistic observation.[5]

2 SIGNAL PS

In this section, we derive the PS (auto-correlation PS and cross-correlation PS) of the measured intensity fluctuations and its variance, with an approach similar to Visbal & Loeb (2010). For simplicity, we assume that the detected intensity includes three components: (i) the signal; (ii) the instrumental white noise; (iii) the interloping lines which are redshifted to the same frequency as the signal line, namely

$$I(\Omega, \nu) = I_\alpha(\Omega, \nu) + I_{\mathrm{N}} + \sum_i I_f^i(\Omega, \nu). \tag{1}$$

Throughout this work, we will neglect the possible presence of continuum foregrounds, assuming that they can be easily removed thanks to the smoothness of the frequency spectrum (Wang et al. 2006; Chapman et al. 2015; Wolz et al. 2015).

Note that the comoving coordinates are related to angle and frequency displacement from an arbitrary origin, $\boldsymbol{x}^0$, as follows:

$$x_1, x_2 = \chi(z_\alpha)\Delta\theta + x_1^0, x_2^0 \tag{2}$$

$$x_3 = \frac{\mathrm{d}\chi}{\mathrm{d}\nu}\Delta\nu + x_3^0, \tag{3}$$

where $\chi(z_\alpha)$ is the comoving distance from the observer to the signal, $\mathrm{d}\chi/\mathrm{d}\nu = c(1 + z_\alpha)[H(z_\alpha)\nu]^{-1}$, $(\Delta\theta, \Delta\nu)$ are the displacements in angle and frequency from the origin $\boldsymbol{x}^0$ (centre of the survey). In this process, a subtlety arises (Visbal & Loeb 2010; Gong et al. 2014) because I_f^i is not emitted at z_α. Therefore, in that term, we

[5] We assume a flat Λcold dark matter cosmology compatible with the latest Planck results: $h = 0.677$, $\Omega_{\mathrm{m}} = 0.31$, $\Omega_{\mathrm{b}} = 0.049$, $\Omega_\Lambda = 1 - \Omega_{\mathrm{m}}$, $n = 0.97$, $\sigma_8 = 0.82$ (Planck Collaboration XIII 2015).

should consider coordinates that are the projection at z_α of the real coordinates at z_i:

$$I(\boldsymbol{x}) = I_\alpha(\boldsymbol{x}, z_\alpha) + I_{\rm N} + \sum_i I^i_f \left(x_1 \frac{\chi(z_i)}{\chi(z_\alpha)}, x_2 \frac{\chi(z_i)}{\chi(z_\alpha)}, x_3 \frac{(1+z_i)H(z_\alpha)}{(1+z_\alpha)H(z_i)}, z_i \right), \quad (4)$$

where $1 + z_i = (1 + z_\alpha)\lambda_\alpha/\lambda_i$.

When considering the Fourier transform of the fluctuations, this projection introduces (i) a global extra factor that multiplies the PS; (ii) anisotropies due to the different projection of modes along and across the line of sight; (iii) a loss of correspondence between comoving and observed k-modes:

$$\delta I(\boldsymbol{k}) = \overline{I}_\alpha \langle b \rangle_\alpha \delta^\alpha_{\boldsymbol{k}} + \delta^N_{\boldsymbol{k}} + \sum_i C(z_i) \overline{I}^i_f \langle b \rangle_i \delta^i_{\boldsymbol{k}'(\boldsymbol{k})}; \quad (5)$$

where $\overline{I}$ and $\langle b \rangle$ with each subscript are the mean intensity and halo luminosity-weighted mean bias of each line; $\delta^N_{\boldsymbol{k}}$ is the instrumental noise (see Section 3). The global extra factor is

$$C(z_i) = \left(\frac{\chi(z_\alpha)}{\chi(z_i)} \right)^2 \frac{(1+z_\alpha)H(z_i)}{(1+z_i)H(z_\alpha)}; \quad (6)$$

$$\boldsymbol{k}'(\boldsymbol{k}) = \left(k_1 \frac{\chi(z_\alpha)}{\chi(z_i)}, k_2 \frac{\chi(z_\alpha)}{\chi(z_i)}, k_3 \frac{(1+z_\alpha)H(z_i)}{(1+z_i)H(z_\alpha)} \right). \quad (7)$$

From the above equations, the PS of the measured intensity fluctuations becomes

$$P(\boldsymbol{k}) = \langle \delta I(\boldsymbol{k}) \delta I^*(\boldsymbol{k}) \rangle = P_\alpha(\boldsymbol{k}) + P_{\rm N} + \sum_i P^i_f \quad (8)$$

where

$$P_\alpha(\boldsymbol{k}) = \overline{I}_\alpha{}^2 \langle b \rangle^2_\alpha P_{\rm dm}(\boldsymbol{k}, z_\alpha),$$

$$P_{\rm N} = \langle \delta^{\rm N} \delta^{\rm N} \rangle,$$

$$P^i_f(\boldsymbol{k}) = C(z_i) \left(\overline{I}^i_f \right)^2 \langle b \rangle^2_i P_{\rm dm}(\boldsymbol{k}', z_i),$$

in deriving the last line, the relation $\langle \delta_{\boldsymbol{k}'(\boldsymbol{k})} \delta_{\boldsymbol{p}'(\boldsymbol{p})} \rangle = C^{-1} P_{\rm dm}(\boldsymbol{k}') \delta^3(\boldsymbol{k} - \boldsymbol{p})$ is used and $P_{\rm dm}$ is the dark matter PS. The noise component $P_{\rm N}$ is well known and easily subtracted; the interlopers power spectrum, $P^i_f(\boldsymbol{k})$, is, however, unknown and yet must be removed in order to extract the astrophysical PS signal.

The variance of $P(\boldsymbol{k})$ is

$$\sigma^2_{\rm P}(\boldsymbol{k}) = \delta P^2(\boldsymbol{k}) = \langle \left(\delta I(\boldsymbol{k}) \delta I^*(\boldsymbol{k}) \right)^2 \rangle - \langle \delta I(\boldsymbol{k}) \delta I^*(\boldsymbol{k}) \rangle^2. \quad (9)$$

Using the fact that noise and interloping lines only correlate with themselves, and that $\langle | \delta_{\boldsymbol{k}} |^4 \rangle = 2\sigma^4_{\boldsymbol{k}}$ and $\langle |\delta^{\rm N}|^4 \rangle = 2P^2_{\rm N}$, it is easy to prove (see Appendix A for the full calculation)

$$\sigma^2_{\rm P}(\boldsymbol{k}) = \left[P_\alpha(\boldsymbol{k}) + P_{\rm N} + \sum_i P^i_f(\boldsymbol{k}) \right]^2. \quad (10)$$

From this equation, we can see that the variance depends strongly on the detector noise and on the PS of the interloping lines.

In case the PS is isotropic, $P(\boldsymbol{k}) = P(k)$, several independent modes can be combined to reduce the PS variance at given k:

$$P(k) = \left(\sum_k \frac{1}{\sigma^2_{\rm P}(\boldsymbol{k})} \right)^{-1} \sum_k \frac{P(\boldsymbol{k})}{\sigma^2_{\rm P}(\boldsymbol{k})}, \quad (11)$$

where the sum is over all the modes with $|\boldsymbol{k}| = k$.

In order to estimate the S/N, we have to consider the PS variance due to the finite survey volume and resolution. In this case, the probed k-modes are discrete and multiples of $(2\pi/L_1, 2\pi/L_2, 2\pi/L_3)$, where L_1, L_2, L_3 are the dimensions of the survey volume. Suppose the survey has a resolution $l_\parallel$ and $l_\perp$ along and perpendicular to the line of sight (generally $l_\parallel \gg l_\perp$), respectively, then, only modes satisfying $2\pi/L_1, 2\pi/L_2 < k_1, k_2 < 2\pi/l_\perp$ and $2\pi/L_3 < k_3 < 2\pi/l_\parallel$ are accounted.

Sometimes it is useful to estimate the total PS variance and S/N for all modes with $k_{\rm min} < k < k_{\rm max}$ (Pullen et al. 2014):

$$\langle \sigma^2_{\rm P} \rangle = \left(\int \frac{d^3k}{\Delta k^3} \frac{1}{\sigma^2_{\rm P}(\boldsymbol{k})} \right)^{-1}; \quad (12)$$

$$\langle ({\rm S/N})^2 \rangle = \int \frac{d^3k}{\Delta k^3} \left(\frac{P(\boldsymbol{k})}{\sigma_{\rm P}(\boldsymbol{k})} \right)^2, \quad (13)$$

where $\Delta k^3 = (2\pi)^3/V_{\rm s}$ is the k-space volume occupied by each discrete mode and the integral is over all wavenumbers with $k_{\rm min} < | \boldsymbol{k} | < k_{\rm max}$, $k_1, k_2 < 2\pi/l_\perp$ and $k_3 < 2\pi/l_\parallel$.

The contamination in the auto-correlation PS (equation 8) could be suppressed by cross-correlating different measurements targeting two different signals, α and β, that are contaminated by uncorrelated interloping lines (Visbal & Loeb 2010). The cross-correlation PS is (Visbal & Loeb 2010):

$$P_{\alpha,\beta}(\boldsymbol{k}) = \langle I_\alpha \rangle \langle b \rangle_\alpha \langle I_\beta \rangle \langle b \rangle_\beta P_{\rm dm}(\boldsymbol{k}), \quad (14)$$

where only the signal term is left as noise and interloping terms are uncorrelated for α and β. Nevertheless, noise and interloping lines increase the variance:

$$\sigma^2_{P\alpha\beta} = \frac{1}{2} \left[P^2_{\alpha\beta} + \left(P_\alpha + P_{N,1} + \sum_i P^i_{f,1} \right) \left(P_\beta + P_{N,2} + \sum_i P^i_{f,2} \right) \right], \quad (15)$$

where the subscripts 1, 2 represent the qualities in the two measurements, respectively. We will apply this suppression method to our model and discuss more specific details in Section 5.

3 LINE DETECTABILITY

We start by assessing first the detectability of the Lyα PS without considering the interlopers contamination. Our discussions are based on different setup parameters of a small space telescope that can map efficiently a large sky area in the visible (corresponding to $2.2 < z_\alpha < 4.8$) and NIR ($z > 4.8$) spectral bands. We do not aim at proposing an optimal setup of such instrument, but rather at understanding to what extent the Lyα IM is a viable tool for studying high-z galaxies.

The size of the voxel is one of the most relevant factors for detectability. The voxel size along the line of sight is given by $l_\parallel = \frac{dl}{dz} \Delta z = \frac{c(1+z)}{H(z)R}$; in the perpendicular direction, it is instead $l_\perp = \chi(z)\theta_{\rm min}$. As such, it depends on the spectral resolution, R, and angular resolution, $\theta_{\rm min}$, of the telescope. The choice of an optimal $l_\parallel$ and $l_\perp$ is crucial: a small voxel results in a smaller volume loss following interlopers removal but requires a longer time to complete a survey for a given area; large voxels suffer from the opposite problem. Moreover, as we will discuss in Section 4, there are additional limitations imposed by the ancillary imaging survey used to identify the interlopers. The latter sets the minimum voxel size to the precision of the redshift measurement (i.e. typically

$\approx 0.05(1+z)$ for photometric surveys) along the line of sight. It is necessary to find a balanced choice that is specific to the IM experiment configuration and goals.

Our fiducial instrument has a $\theta_{\rm min} = 6$ arcsec beam full width at half-maximum, a spectrometer with resolution $R = \lambda/\Delta\lambda = 100$ and a survey area of 250 deg^2 (Silva et al. 2013; Doré et al. 2014; Pullen et al. 2014; Cooray et al. 2016). Therefore, the sample space has voxels with $\Delta l_{\parallel} = 35.3$ and 28.1 Mpc, and $\Delta l_{\perp} = 214$ and 257 kpc, for $z = 4$ and 7, respectively.

In our setup, the voxel size is always larger than the galaxy correlation length (typically $\approx$1 Mpc[3]); therefore, we expect that each voxel contains several galaxies. Also, as $\Delta l_{\parallel} \gg \Delta l_{\perp}$ (typically $\approx$20–30 Mpc versus $\approx$200–300 kpc), only transversal modes contribute to the PS measurement at $k > 0.1\,h\,{\rm Mpc}^{-1}$.

Another relevant crucial point is the instrumental noise. A space telescope is usually background-limited, i.e. the noise level[6] is set by Poisson fluctuations of the background light. For Lyα observations, the most important background is the Zodiacal Light (ZL). In this case,

$$\sigma_{\rm N} \approx 1.37\,\epsilon^{-1/2}\,{\rm nW\,m^{-2}\,sr^{-1}} \times \left[\frac{\mu{\rm m}}{\lambda}\,\frac{R}{100}\,\frac{I_{\rm ZL}}{10^3{\rm nW\,m^{-2}\,sr^{-1}}}\,\frac{0.126{\rm m}^2}{\pi D^2/4}\,\frac{8.5\times10^{-10}\,{\rm sr}}{\Omega_{\rm pix}}\,\frac{10^5\,{\rm s}}{t_{\rm obs}}\right]^{1/2}, \quad (16)$$

where $I_{\rm ZL} = \nu I_{\nu} \approx 10^{2-3}\,{\rm nW\,m^{-2}\,sr^{-1}}$ is the typical ZL flux in the relevant frequency range (Kashlinsky 2005; Doré et al. 2014) and D is the diameter of the telescope. An efficiency ϵ is added to account for the photons loss by mirrors and integral field unit, here assumed conservatively to be $\epsilon = 0.25$.

3.1 PS observations

The first generation of intensity mappers are likely to have a limited S/N that will allow only to probe EoR Lyα fluctuations PS. In this section, we discuss an instrument designed for this aim. Nevertheless, in the future, more powerful instruments could undertake tomographic observations and we will discuss such possibility in Section 3.2.

The PS of the instrumental noise is

$$P_{\rm N}(z) = \sigma_{\rm N}^2 V_{\rm pix}, \quad (17)$$

where $\sigma_{\rm N}$ is from equation (16) and $V_{\rm pix}$ is the comoving voxel volume. We then compute the S/N using $\sigma_{\rm P}^2 = (P_{\alpha} + P_N)^2$ and equation (13) (we use $\Delta z = 1$ for the survey volume $V_{\rm s}$ and divide k-space in k-bins with $\Delta k = 1.2k$).

A telescope with a field of view of $\approx$20–30 deg^2 (similar to the proposed SPHEREx; see Doré et al. 2014) can observe a field of 200–250 deg^2 in two years, with exposure time $t_{\rm obs} \approx 10^7$ s per pointing. Here we consider a more conservative setup with $t_{\rm obs} = 10^5$ s, which is more feasible as it only takes several days to complete the survey.

Fig. 1 shows the Lyα PS from $z = 7$, and the corresponding S/N assuming 10^5 s exposure time per pointing and a 250 deg^2 survey area.[7] The S/N is proportional to the number of probed modes: it

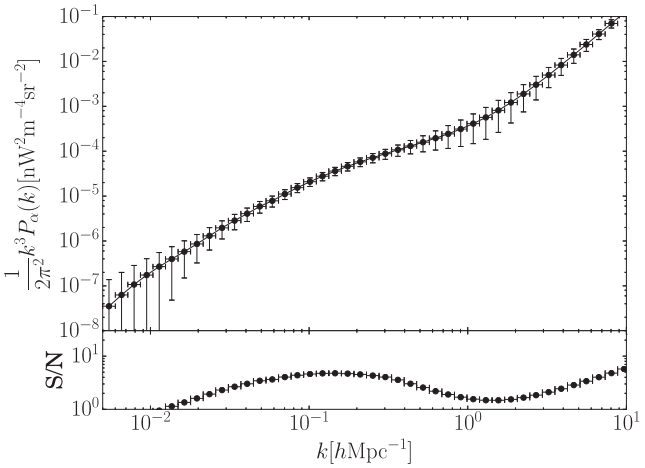

Figure 1. Top: predicted Lyα power spectrum from $z = 7$ with error bars; Bottom: S/N in each k-space bin. The S/N is computed for a background-limited NIR telescope with diameter $D = 0.4$ m, angular and spectral resolution ($\delta\theta = 6$ arcsec, $R = 100$), exposure time 10^5 s per pointing and a survey area of 250 deg^2. Each bin has a width $\Delta k = 1.2k$.

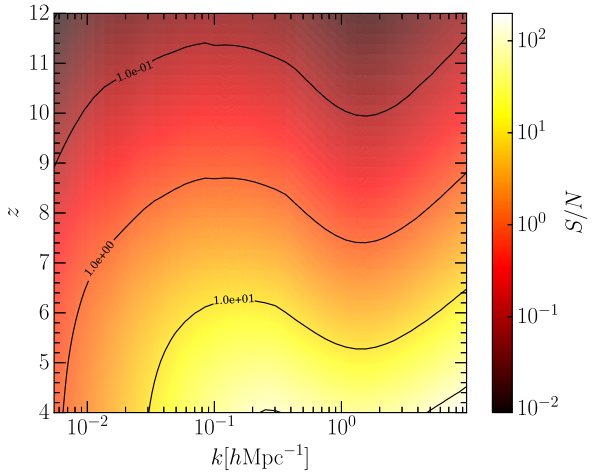

Figure 2. The S/N of the observed PS as function of redshift z and wavenumber k; the observational setup is the same of Fig. 1.

scales as k^3 for bins with $k \lesssim 0.1\,h\,{\rm Mpc}^{-1}$ and as k^2 for smaller scales, due to the limited spectroscopic resolution. This transition generates a decreasing S/N for $0.1\,h\,{\rm Mpc}^{-1} \lesssim k \lesssim 1\,h\,{\rm Mpc}^{-1}$, where the PS is steeper than k^{-2}. Above $k \sim 1\,h\,{\rm Mpc}^{-1}$, the S/N increases again because shot noise dominates and PS is constant. However, as discussed in CF16, shot noise on the $\sim$Mpc scale might be suppressed by Lyα diffusion in the IGM, and therefore the S/N can be overestimated in that range. We conclude that Lyα IM is best suited to study fluctuations in the linear regime on scales $\sim$10 Mpc. These results are encouraging because they show that Lyα IM from the late EoR can be detected, provided that continuum foregrounds and low-redshift interlopers can be efficiently removed.

Fig. 2 shows a more general dependence of S/N on wavenumber k for Lyα signals coming from different redshifts. The observational setup is the same as in Fig. 1. We find that the Lyα PS is accessible to this kind of observations at least for the late EoR (i.e. S/N $\approx$5 at $k = 0.1\ h\ {\rm Mpc}^{-1}$ for $z \sim 7$).

We then investigate how the detectability depends on varying exposure time $t_{\rm obs}$, using the total S/N, computed using equation (13),

[6] We ignore dark current and readout noise as they depend strongly on survey implementation; This approximation is safe at least for instruments similar to SPHEREx (Zemcov, private communication).

[7] This survey set-up is rather conservatively; a deeper survey should be possible.

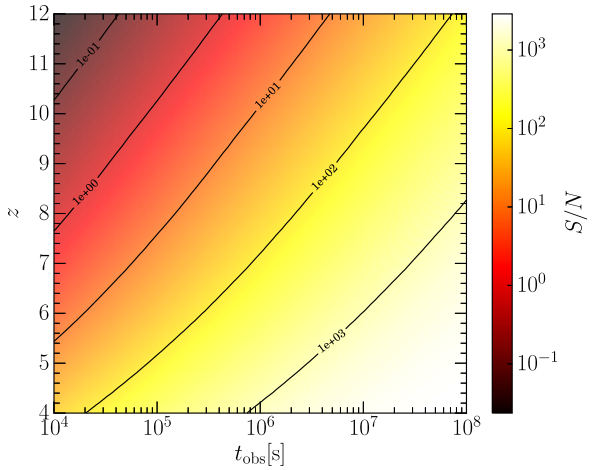

Figure 3. Total S/N for detection of Lyα fluctuations; the observational setup is the same of Fig. 1.

in the range $5 \times 10^{-3}\,h\,\mathrm{Mpc}^{-1} < k < 2\,h\,\mathrm{Mpc}^{-1}$ as the indicator. The results are plotted in Fig. 3. From there, we see that a detection of Lyα PS with low S/N is at reach even at $z > 7$. This formalism also allows us to find the best observational strategy for a PS observation: given a fixed total observing time, we want to find the optimal exposure time per pointing. Considering only the instrumental noise, from equations (13), (16) and (17), we have

$$(\mathrm{S/N})^2 \propto \frac{A_{\mathrm{surv}}}{\sigma_N^2}. \tag{18}$$

Since $A_{\mathrm{surv}} \propto t_{\mathrm{obs}}^{-1}$ and $\sigma_N^2 \propto t_{\mathrm{obs}}^{-1}$, the S/N does not depend on the depth of the survey as long as the cosmic variance term negligibly appears in equation (10). In other words, the best strategy for an IM experiment is to carry out a shallow, however, large area survey.

In practice, though, the optimal t_{obs} is set by the technical implementation of the survey, which should take into account the following limitations: (i) t_{obs} cannot be shorter than, or even comparable to, the instrumental pointing time; (ii) with a large survey area, it is impossible to avoid sky regions with higher foregrounds; (iii) as we will discuss in Section 4, the IM survey might need deep ancillary galaxy surveys for interloper removal, and therefore the data available for final analysis are limited to the overlapping sky regions.

3.2 Tomography

Alternatively, an IM experiment allows us to make tomographic maps of the Lyα intensity, although only the low-z part of the signal is accessible to the fiducial space telescope design introduced above.

In CF16, we found that the mean Lyα intensity at $z = 4$ is $I_\alpha \approx 0.1\,\mathrm{nW\,m^{-2}\,sr^{-1}}$. At the same redshift, the dark matter field has a fluctuations level of $\sigma_{\mathrm{dm}} \approx 0.23$ on 10 Mpc scales, and the mean Lyα bias $\langle b\rangle_\alpha \approx 3$. Therefore, if the survey has voxels of volume $(10\,\mathrm{Mpc})^3$, corresponding to $R \approx 350$ and $\Delta\theta_{\mathrm{pix}} = 4.7$ arcmin at $z = 4$, the 1σ Lyα fluctuations level is

$$\sigma_\alpha = I_\alpha \langle b\rangle_\alpha \sigma_{\mathrm{dm}} \approx 0.07\ \mathrm{nW\,m^{-2}\,sr^{-1}}, \tag{19}$$

which is larger than the noise level $\sigma_{\mathrm{N}} \approx 0.04\ \mathrm{nW\,m^{-2}\,sr^{-1}}$ in equation (16) for $t_{\mathrm{obs}} = 10^6$ s. Therefore, even this small intensity mapper can observe directly the spatial fluctuations of Lyα emission from low-redshift galaxies, although with a modest S/N.

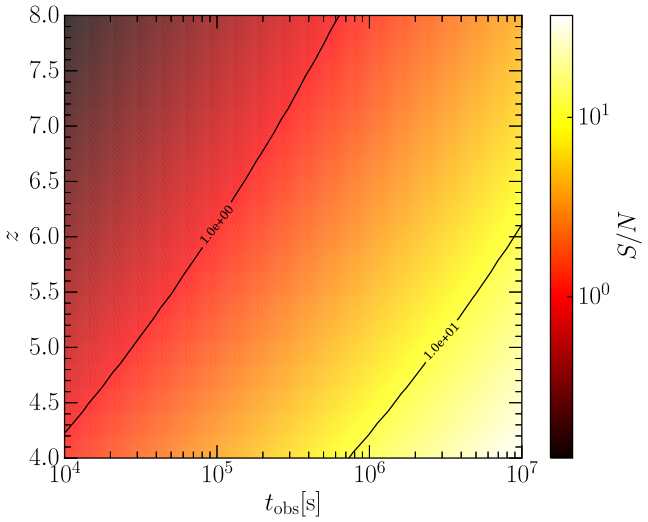

Figure 4. The S/N of tomographic observations for a voxel size $(10\,\mathrm{Mpc})^3$. The S/N is computed for a background-limited NIR telescope with diameter $D = 2$ m, angular and spectral resolution ($\delta\theta = 4.7$ arcsec, $R = 350$).

The tomographic observation of the Lyα signal from the EoR is more challenging, as the Lyα intensity drops by one order of magnitude. Thus, a tomographic map of the EoR signal requires a more powerful instrument. Fig. 4 shows the $\mathrm{S/N} = \sigma_\alpha/\sigma_{\mathrm{N}}$ as a function of z and t_{obs} for a 2 m space telescope and same voxels of $(10\,\mathrm{Mpc})^3$ volume. The observation requires an integration time of at least a few months and even so, it will be only feasible for the late stages of the EoR. The experiment can be even more challenging once the confusion by interloping lines such as Hα and [O II] that dominate over Lyα emission are accounted for.

4 INTERLOPING LINES

Low-redshift emission lines could significantly contribute to the observed intensity fluctuations (see equation 8). Particularly important for Lyα experiments are the Hα (0.6563 μm), [O III] (0.5007 μm) and [O II] (0.3727 μm) (Gong et al. 2014; Pullen et al. 2014) lines. Their power spectra may dominate the Lyα signal, and are distorted and amplified due to coordinate projection effects. Their contribution must therefore be accurately removed from the received flux. In what follows, we investigate the power spectra of these interloping lines and suggest a technique to remove them.

4.1 Power spectra of interloping lines

The abundance matching technique required to compute the PS of interloping lines involves the knowledge of the line LF, which is not as easy as the continuum LF to measure. Fortunately, our Lyα signal is only contaminated by interlopers at low redshift ($z < 2$), where observations are more easily available. We use the Schechter LF parametrization (Schechter 1976) in Ly et al. (2007) and Drake et al. (2013) (see Table 1). The intrinsic intensity of interlopers is not relevant in our work, therefore we use the unprocessed LF, i.e. without dust correction.

Currently, the observed interloper LFs are not complete enough to derive a redshift evolution. This forces us to use the

Table 1. Schechter parameters of the observed LF used in this work. Data are from Ly et al. (2007) (L07) and Drake et al. (2013) (D13); for simplicity, we consider only works that fitted their LF with a Schechter function, neglecting, for example, Gunawardhana et al. (2013). We use the raw LF, without dust correction.

Hα	z	ϕ	$L_\star$	α
L07	0.24	-2.98 ± 0.40	41.25 ± 0.34	-1.70 ± 0.10
	0.4	-2.40 ± 0.14	41.29 ± 0.13	-1.28 ± 0.07
D13	0.25	-2.43 ± 0.19	40.83 ± 0.18	-1.03 ± 0.16
	0.4	-2.44 ± 0.16	41.16 ± 0.12	-1.14 ± 0.14
	0.5	-2.23 ± 0.11	41.24 ± 0.08	-1.23 ± 0.13
[O II]	z	ϕ	$L_\star$	α
L07	0.89	-2.25 ± 0.13	41.33 ± 0.09	-1.27 ± 0.14
	0.91	-1.97 ± 0.09	41.40 ± 0.07	-1.20 ± 0.10
	1.18	-2.20 ± 0.10	41.74 ± 0.07	-1.15 ± 0.11
	1.47	-1.97 ± 0.06	41.60 ± 0.05	-0.78 ± 0.13
D13	0.35	-2.31 ± 0.24	40.90 ± 0.18	-1.06 ± 0.36
	0.53	-2.85 ± 0.35	41.13 ± 0.20	-1.68 ± 0.36
	1.19	-2.41 ± 0.08	41.61 ± 0.07	-0.95 ± 0.14
	1.46	-2.03 ± 0.05	41.76 ± 0.05	-0.91 ± 0.11
	1.64	-1.68 ± 0.47	41.73 ± 0.11	-0.91 ± 0.11
[O III]	z	ϕ	$L_\star$	α
L07	0.48	-2.55 ± 0.25	41.17 ± 0.22	-1.49 ± 0.11
	0.42	-2.38 ± 0.22	41.11 ± 0.24	-1.25 ± 0.13
	0.62	-2.58 ± 0.17	41.51 ± 0.15	-1.22 ± 0.13
	0.83	-2.54 ± 0.50	41.53 ± 0.11	-1.44 ± 0.09
D13	0.14	$-3.67 \pm \infty$	$41.6 \pm \infty$	-1.63 ± 0.42
	0.63	-2.57 ± 0.12	41.44 ± 0.09	-1.27 ± 0.11
	0.83	-2.25 ± 0.80	41.28 ± 0.09	-0.76 ± 0.21
	0.99	-3.00 ± 0.23	41.70 ± 0.13	-0.78 ± 0.20

Table 2. Mean Schechter parameters of the interopers LF from Table 1.

Hα	ϕ	$L_\star$	α	$\langle z \rangle$
	-2.36 ± 0.07	41.19 ± 0.06	-1.33 ± 0.05	0.4
O II	ϕ	$L_\star$	α	$\langle z \rangle$
	-2.10 ± 0.03	41.61 ± 0.02	-1.05 ± 0.04	1.19
O III	ϕ	$L_\star$	α	$\langle z \rangle$
	-2.58 ± 0.07	41.43 ± 0.05	-1.30 ± 0.05	0.72

variance-weighted mean Schechter parameters[8] to construct the $L = L(M)$ relations at the variance-weighted mean redshift. The same relation is then applied to all redshifts (see CF16). The mean Schechter parameters and redshifts are listed in Table 2. In this scenario, the redshift evolution of the LF is purely attributed to the halo mass function evolution. Although this might seem a strong assumption, the redshift intervals[9] of the interloper lines that we need to consider are relatively small. For example, for the Hα line (the strongest contributor), the relevant interval is $0.30 < z < 0.67$. As a result, we believe that the assumption does not affect our conclusions.

Fig. 5 shows the PS of interlopers compared with Lyα from $z = 7$. As we discuss in Section 2, incorrectly projecting the interlopers to higher redshift introduces distortions that can amplify their PS. Since the projected interlopers PS is anisotropic, we average it over the solid angle, $P(k) = \frac{1}{4\pi} \int \mathrm{d}\Omega P(\boldsymbol{k})$. However, the anisotropy information can be used to assess the quality of the removal procedure (Gong et al. 2014). We find that interlopers dominate the PS by one to two orders of magnitude on all scales, and that Hα is the dominant confusion source. Therefore, an appropriate removal of the interloping PS from Lyα signal, discussed in the following, is crucial.

4.2 Interlopers removal

Removing the interloping lines requires a strategy that is different from that used to deal with continuum foregrounds. A possible strategy is to mask the contaminated pixels (Gong et al. 2014; Pullen et al. 2014; Breysse et al. 2015). This is feasible because the galaxy population emitting the interloping lines is very different from the signal sources at EoR: bright galaxies are very rare at high redshift because they are exponentially suppressed in the LF. Hence, if we remove the most luminous pixels from the survey, most of them would be occupied by low-z galaxies and the intensity of interloping lines could be reduced significantly.

However, although straightforward, this approach has two drawbacks: (i) if the S/N of the observation is not high, bright voxels can result from noise or foreground fluctuations; (ii) it removes also Lyα flux (Breysse et al. 2015). For this reason, in this work, we will use a different approach relying on ancillary galaxy surveys for the identification of the interlopers (Pullen et al. 2014; Silva et al. 2015; Yue et al. 2015). This strategy would affect only weakly the Lyα PS; however, ancillary surveys have to be sufficiently deep and wide. Moreover, photometric redshifts have to be precise because photometric estimates are expected to be more uncertain than the IM redshift resolution. To clean the IM map, it is necessary to discard multiple voxels per interloper (e.g. for an IM survey with $R = 100$ and a galaxy survey with 5 per cent redshift uncertainty, 5 voxels have to be discarded for each interloper).

To demonstrate the feasibility of such approach, we first perform a calculation similar to that shown in the left-hand panel of Fig. 5 but imposing an upper limit to the mass of the interloping galaxies. We assume that the pixels containing galaxies larger than this upper limit are removed from the survey. Fig. 5 (right) shows the PS of Lyα signal at $z = 7$ and interlopers, normalizing all power spectra at $k = 0.1\,h\,\mathrm{Mpc}^{-1}$. Both the mean intensity, the mean bias and the shot noise depend on the upper limit ($2 \times 10^{11}\,\mathrm{M}_\odot$ for Hα, $4.4 \times 10^{11}\,\mathrm{M}_\odot$ for [O II], and $2 \times 10^{12}\,\mathrm{M}_\odot$ for [O III]). Removing massive galaxies suppresses very efficiently the PS of the interlopers. We find that the removed voxels occupy only 2 per cent of the survey volume.

In the left-hand panel of Fig. 6, we show the minimum mass of haloes that has to be removed from the survey to reach a interloper-to-signal ratio r (defined as the PS ratio at scale $k = 0.1\,h\,\mathrm{Mpc}^{-1}$) for PS of Lyα from redshift z. We find that an effective interloper removal requires to resolve galaxies hosted by haloes with $M \gtrsim 10^{11}\,\mathrm{M}_\odot$ and line flux $f \gtrsim 10^{-16}\,\mathrm{erg\,cm}^{-2}$. This can be challenging for a large area survey. The fraction of the volume loss can be substantial, as shown by the right-hand panel of Fig. 6 when considering a 5 per cent ($R = 20$) redshift uncertainty in the ancillary galaxy survey, resulting in more than one voxel discarded per galaxy. We remind that if more than ∼30 per cent of the survey volume is masked, the PS reconstruction can be unfeasible (Kashlinsky et al. 2005). From the right-hand panel of Fig. 6, we conclude that cleaning a Lyα IM survey can be intrinsically difficult at $z > 12$,

[8] The results in Section 4.2 do not depend strongly on this choice. We checked that, using several combinations of the observed LF in Table 1, our qualitative conclusions do not change.

[9] The emission redshift is $1 + z_{\rm em} = (1 + z)(\nu_{\rm int}/\nu_\alpha)$, therefore at $z_\alpha = 6, 7, 8$, the corresponding emission redshifts for the interlopers are $z_{\rm H\alpha} = 0.30, 0.48, 0.67$, $z_{\rm O\,II} = 1.28, 1.61, 1.94$ and $z_{\rm O\,III} = 0.70, 0.94, 1.19$.

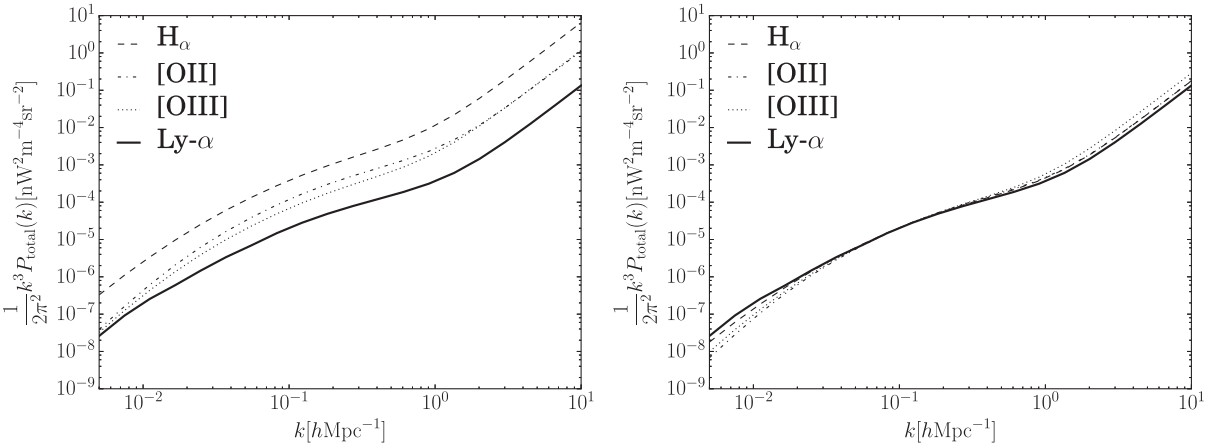

Figure 5. Left: comparison of the interlopers and Lyα power spectra at $z = 7$. Right: same after bright interlopers removal.

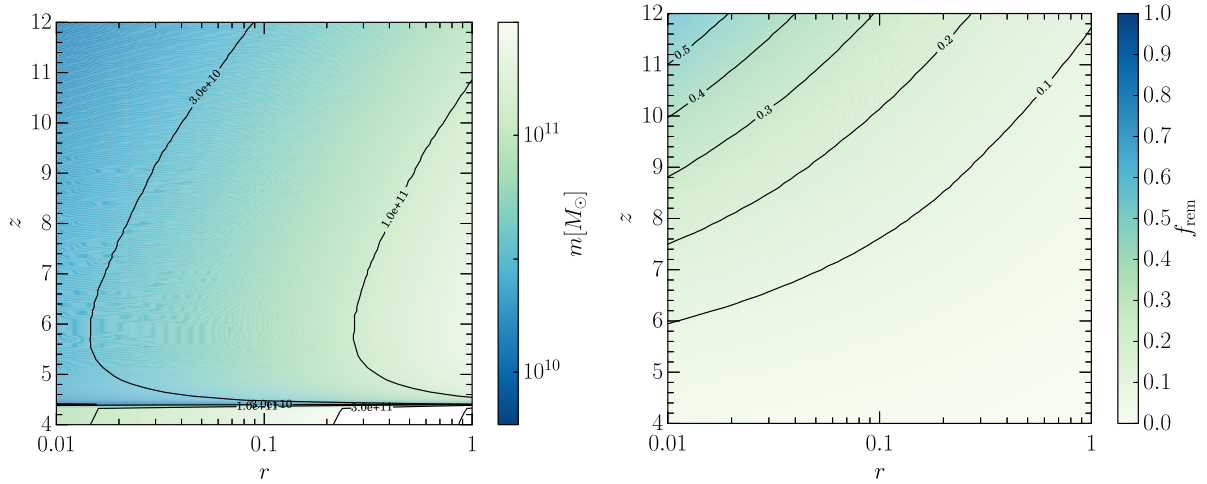

Figure 6. Left: maximum mass of the galaxies contributing to the interlopers PS. The sharp discontinuity at $z = 4.4$ is due to the Hα line entering the survey. Right: fraction of voxels that has to be removed to obtain a ratio r between the interlopers and Lyα PS on scale $k = 0.1\,h\,{\rm Mpc}^{-1}$ at redshift z. A redshift uncertainty in the ancillary galaxy survey of 5 per cent ($R = 20$) has been assumed, thus multiple voxels are discarded for each interloper.

while the volume loss is not problematic for observations at later epochs.

We can then translate the above constraints on a limiting apparent magnitude at which interloper galaxies must be removed. To this aim, we use the optical and NIR rest-frame LFs in Helgason, Ricotti & Kashlinsky (2012) and assign luminosities to DM haloes using the abundance matching technique. The apparent AB magnitude at a specified wavelength is obtained from linear interpolation between two neighbouring bands in Helgason et al. (2012). Fig. 7 shows the maximum depth needed by a survey to remove interlopers as a function of r and signa redshift in the Y, J, H and K bands. To access the signal from late EoR the ancillary survey must reach an AB mag $\gtrsim 26$.

Compared with the designed sensitivity of future photometric surveys, this is rather challenging. For example, the *Euclid*[10] wide survey will reach a limiting magnitude of 24 in bands Y, J and H: this can be enough only to clean the Lyα PS at $z < 4.4$ (without the Hα line). Observing the EoR signal and reaching AB mag $m = 27$–28 is extremely challenging and is at the edge of the capabilities of future instruments, such as *Wide-Field Infrared Survey Telescope*[11] or FLARE. These results are model-dependent because the EoR Lyα PS is not constrained; if the Lyα PS is 10 times weaker than CF16, EoR science will be completely out of reach even for the next generation of galaxy surveys.

5 CROSS-POWER SPECTRA

In Section 4.2, we have discussed an interloper removal method based on ancillary surveys. In spite of the optimistic assumptions (for example, we have neglected the scatter in the line luminosity, SFR and halo mass relations), the required masking depth is relatively demanding.

An alternative strategy would be to use the cross-correlation between two different IM experiments contaminated by different interloping lines. The 157.7 μm [C II] fine structure line is the brightest of all the metal lines, contributing generally up to ∼1 per cent of the total galaxy IR luminosity. Its line luminosity scales tightly with the SFR, but is affected also by the ISM metallicity (Vallini et al. 2013, 2015). The removal of continuum foreground and interloping

[10] http://sci.esa.int/euclid/

[11] http://wfirst.gsfc.nasa.gov

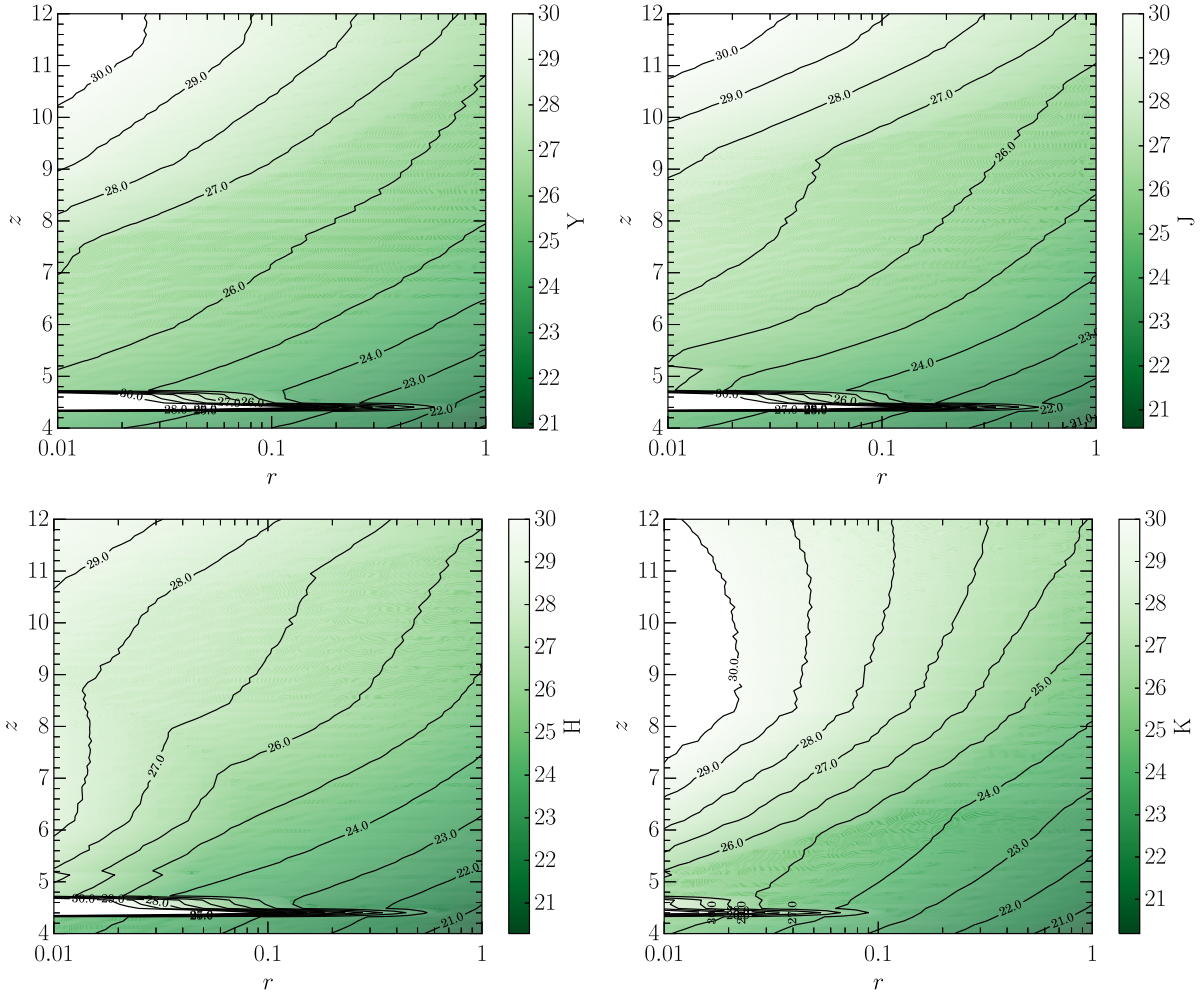

Figure 7. Limiting magnitude in different spectral bands (Y, J, H, K) required for a survey to clean the Lyα PS signal from interlopers; r is the ratio between the interlopers and Lyα PS on scale $k = 0.1\,h\,\mathrm{Mpc}^{-1}$ at redshift z. The sharp horizontal feature at $z = 4.4$ is due to the Hα PS from $z = 0$; it formally diverges (see equation 6).

lines for [C II] auto-correlation PS measurements was investigated in Yue et al. (2015). In this section, we investigate its cross-correlation with the Lyα line using the [C II] model from Yue et al. (2015). The interloping lines for these two signals are not correlated with each other because they are produced in non-overlapping redshift intervals.

5.1 [C II] line intensity and cross-power

The mean [C II] intensity can be directly obtained from the galaxy line luminosity (CF16):

$$I_{\mathrm{C\,II}}(z) = \frac{c}{4\pi\nu_{\mathrm{C\,II}}H(z)}\int \mathrm{d}M\,\frac{\mathrm{d}n}{\mathrm{d}M}L_{\mathrm{C\,II}}(M,z). \tag{20}$$

where $L_{\mathrm{C\,II}}(M, z)$ is from the model in Yue et al. (2015). It spatially fluctuates following the large-scale DM density field multiplied by a line luminosity-weighted mean bias, $\langle b\rangle_{\mathrm{C\,II}}$:

$$\delta I_{\mathrm{C\,II}} = I_{\mathrm{C\,II}}\langle b\rangle_{\mathrm{C\,II}}\delta; \tag{21}$$

where δ is the DM density contrast,

$$\langle b\rangle_{\mathrm{C\,II}} = \frac{1}{\rho_{\mathrm{C\,II}}}\int \mathrm{d}M\,\frac{\mathrm{d}n}{\mathrm{d}M}b(M,z)L_{\mathrm{C\,II}}(M,z). \tag{22}$$

The cross-correlation PS includes three main terms:

(i) Large-scale DM fluctuations originating from the Lyα and [C II] lines, both emitted by the ISM. This component dominates the PS on scales $\gtrsim$1 Mpc. It can be written as

$$P^{\mathrm{s,s}}_{\mathrm{C\,II},\alpha}(k,z) = I_{\mathrm{C\,II}}(z)I^{\mathrm{s}}_{\alpha}(z)\langle b\rangle_{\alpha}\langle b\rangle_{\mathrm{C\,II}}P_{\mathrm{dm}}(k,z), \tag{23}$$

where I^{s}_{α} is the Lyα emission from the ISM;

(ii) Fluctuations from UV continuum emission resulting from the correlation between Lyα emission in the IGM and [C II] emission in the ISM. Lyα fluctuations are produced by (i) UV emission from the galaxies, and (ii) Lyman absorption followed by relaxation in the IGM. We can express the spatial intensity fluctuations as

$$\begin{aligned}\delta I^{\alpha}_{\mathrm{cont}}(z) &= \frac{ch_{\mathrm{P}}\nu_{\alpha}}{4\pi(1+z)}\sum_{n=2}^{\infty}P_{\mathrm{abs}}(n,z)f(n)\\ &\quad\times\int \mathrm{d}z'\frac{\dot{n}_{\nu}(\nu',z')}{H(z')}\prod_{n'=n+1}^{n'_{\max}}T(n',z_{n'})[\langle b(z')\rangle_{\nu'}\delta]\\ &= \frac{1}{4\pi}\int \mathrm{d}\Omega\int_{z}^{+\infty}\mathrm{d}z'A(z,z')\dot{n}_{\nu}(\nu',z')[\langle b(z')\rangle_{\nu'}\delta],\end{aligned} \tag{24}$$

where $P_{\mathrm{abs}}(n, z)$ is the IGM absorption probability of a Lyman-n photon at redshift z, $f(n)$ is the fraction of Lyα photons emitted by

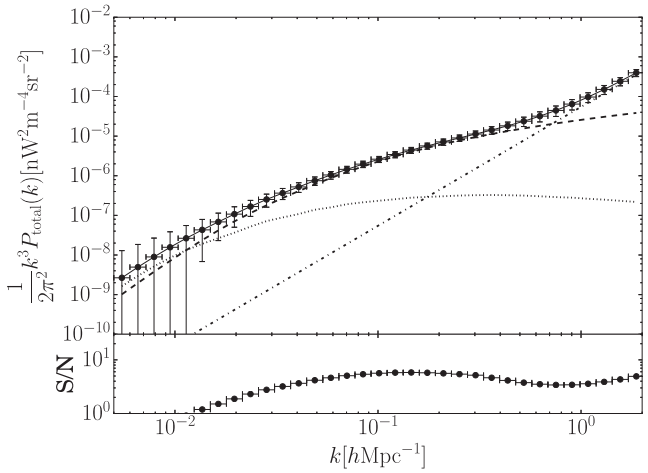

Figure 8. Top: Lyα–[C II] cross-correlation power spectrum at $z = 6$. We show the total PS (solid), large-scale dark matter fluctuations (dashed), fluctuations from UV continuum emission (dot–dashed), and shot noise (see the text). The error bars are computed considering the same [C II] instrumental setup in Yue et al. (2015) and in Section 3.1. Bottom: S/N of the observation as a function of wavenumber.

an H I atom during the decay from the nth energy level, $\dot{n}_\nu$ is the number of UV photons emitted per unit time, volume and frequency, $T(n, z) = 1 - P_{\rm abs}(n, z)$ is the transmission probability; we refer to CF16 for details. The associated cross-correlation PS is

$$P^{\rm s,c}_{{\rm C\,II},\alpha}(k, z) = \left[I_{\rm C\,II}(z)\langle b\rangle_{\rm C\,II} \int_z^{+\infty} {\rm d}z' A(z, z')\dot{n}'_\nu D(z')\frac{\sin(kl')}{kl'} \right] P_{\rm dm}(k, z), \quad (25)$$

where $l'(z, z') = c\int_z^{z'} {\rm d}x\ H(x)^{-1}$ and $D(z')$ is the linear growth factor of perturbations (Mo, van den Bosch & White 2010). It becomes important only on scales $\gtrsim$100 Mpc as fluctuations on scales smaller than the typical mean free path of a photon with energy between the Lyα and the Lyman-limit are washed out.

(iii) Shot noise due to the discrete nature of the sources dominates on small scales:

$$P^{\rm SN}_{{\rm C\,II},\alpha}(k, z) = I_{\rm C\,II} I^{\rm h}_\alpha \frac{1}{\rho^{\rm h}_\alpha \rho_{\rm C\,II}} \int {\rm d}M \frac{{\rm d}n}{{\rm d}M} L_\alpha(M) L_{\rm C\,II}(M); \quad (26)$$

Fig. 8 shows the Lyα–[C II] cross-correlation PS at $z = 6$ with the three main components plotted separately. As expected, the PS is largely dominated by the ISM emission, and only on scales $\gtrsim$100 Mpc the IGM becomes important. We plot also the S/N of an hypothetical observation, using the same [C II] survey proposed in Yue et al. (2015). For consistency, we adopt a spectral resolution $R = 100$ and angular resolution $\Delta\theta = 42$ arcsec for both [C II] and Lyα observations. The total survey area is 250 deg^2, corresponding to about 100 pointings, each with exposure time of 10^5 s (total observing time 10^7s, or about 4 months).

The left-hand panel of Fig. 9 shows the S/N as a function of k and z (assuming $\Delta k = 1.2k$) for the most optimistic case where all interlopers are cleanly removed (equation 15 with $P^i_{f,1} = P^i_{f,2} = 0$). These results are encouraging because they show that, in principle, a Lyα–[C II] IM observation of the late EoR is feasible.

However, as we showed in Section 3.1, interlopers can increase the PS variance well beyond the instrumental noise. For [C II] IM, CO rotational lines (see Bayet et al. 2009; Greve et al. 2014; Popping et al. 2014 for detailed CO emission line studies) are the most important interlopers. They have PS amplitude comparable or even larger than the [C II] one, and therefore they must be removed (see Silva et al. 2015; Yue et al. 2015).

We then added the CO lines (from the model in Yue et al. (2015)), Hα, [O III] and [O II] lines to the variance of the cross-correlation PS (see equation 15). The right-hand panel of Fig. 9 shows the S/N with interlopers (the strong features at $z \approx 4.5$ and 7.2 are due to Hα, CO 2–1 and CO 3–2 lines entering the survey, respectively). The effect of the interlopers is to decrease the S/N significantly; without an efficient removal, the EoR signal is inaccessible. However, compared to the Lyα auto-correlation PS discussed in Section 4.2, the Lyα–[C II] cross-correlation spectrum can be more easily recovered by using a shallower ancillary survey within the capability of a near future instrument. To support this statement, we recompute the S/N, however, removing all the interlopers with $m_{\rm AB} < 24$ (versus ∼26 for recovering the Lyα auto-correlation PS) in the *Euclid* NIR bands (Y, J and H), finding that the recovered signal matches almost perfectly the model without interlopers.

This approach, even though promising, is more difficult to interpret. The information recovered by the cross-PS is degenerate and it is not possible to recover information about Lyα or C II lines individually. It is necessary to rely on ancillary data to extract the relevant astrophysical information, such as a PS measurement of one of the

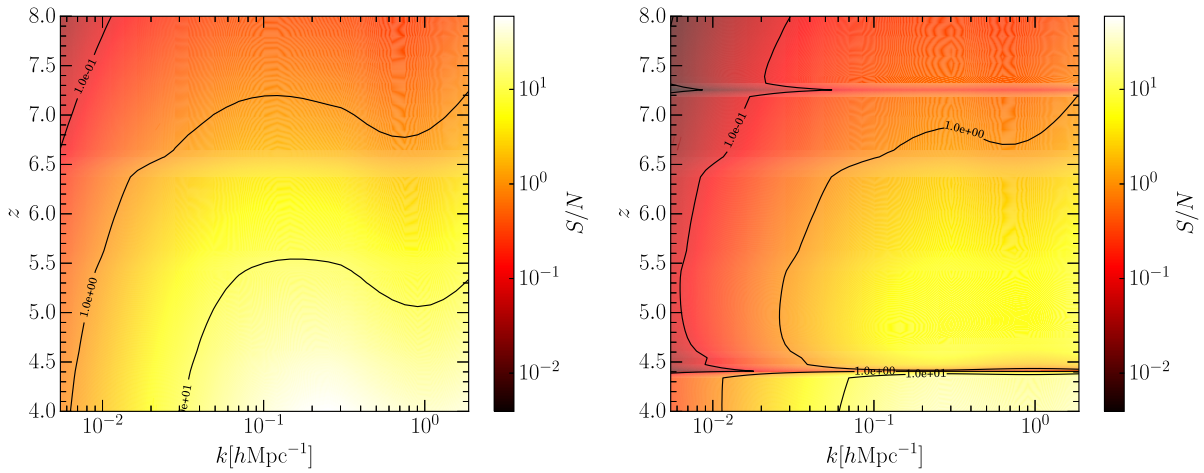

Figure 9. Left: S/N of the Lyα [C II] cross-correlation spectrum versus wavenumber after interloping lines have been removed; Right: same as the left-hand panel, before interloper removal. The observational setup is the same as in Fig. 8.

two lines or a combination of several cross-correlations. Another possibility is to cross-correlate with reserved sources, such as Quasi-stellar object (Croft et al. 2015) or LAE (Comaschi & Ferrara 2016).

6 CONCLUSIONS

We have investigated the feasibility of a Lyman-alpha emitter (Lyα) IM experiment targeting the collective signal from galaxies located at $z > 4$. We have used a recently developed analytical model to predict the Lyα PS, and carefully studied the main observational challenges. These are ultimately quantified by the expected S/N for various observational strategies.

We found that, in principle, the Lyα PS for $z < 8$ is well within the reach of a small space telescope (40 cm in diameter); detections with low S/N are possible only in some optimistic cases up to $z \sim 10$. However, the foreground from interloping lines represent a serious source of confusion and must be removed. The host galaxies of these interloping lines can be resolved via an ancillary photometric galaxy survey in the NIR bands (Y, J, H, K). If the hosts are removed down to AB mag ∼26, then the Lyα PS for $5 < z < 9$ can be recovered with good S/N. We further found that, by cross-correlating the Lyα emission with [C II] emission from the same redshift, the required depth of the ancillary galaxy survey could be within the reach of *Euclid* (AB mag ∼24).

The results of this work show the yet unexplored, remarkable potential of Lyα IM experiments. By using a small space telescope and a few days observing time, it is possible to probe galaxies hosted by DM haloes with $M \approx 10^{10}\,M_{\odot}$ well into the EoR. Such galaxies emit the bulk of the collective Lyα radiation. However, the technical difficulty is represented by the interloping lines removal, which sets demanding requirements to the ancillary survey: the combination of very large survey areas (∼250 deg^2) and significant depth (AB mag ∼26) appear to be challenging also for the next generation telescopes. We have suggested, however, that such problems can be overcome by cross-correlating the Lyα IM with other lines (as the 157.7 μm [C II] fine structure line), thus making a strong synergy between programs targeting different bands almost mandatory.

REFERENCES

Barkana R., Loeb A., 2001, Phys. Rep., 349, 125
Bayet E., Gerin M., Phillips T. G., Contursi A., 2009, MNRAS, 399, 264
Behroozi P. S., Conroy C., Wechsler R. H., 2010, ApJ, 717, 379
Bouwens R. J. et al., 2014a, ApJ, 793, 115
Bouwens R. J., Illingworth G. D., Oesch P. A., Trenti M., Labbe' I., Bradley L., Carollo M., 2014b, ApJ, 803, 34
Bouwens R. J. et al., 2015, ApJ, 803, 34
Breysse P. C., Kovetz E. D., Kamionkowski M., 2014, MNRAS, 443, 3506
Breysse P. C., Kovetz E. D., Kamionkowski M., 2015, MNRAS, 452, 3408
Calvi V. et al., 2016, ApJ, 817, 120
Calzetti D., Armus L., Bohlin R. C., Kinney A. L., Koornneef J., Storchi-Bergmann T., 2000, ApJ, 533, 682
Chapman E. et al., 2015, in Proc. Sci., Cosmic Dawn and Epoch of Reionization Foreground Removal with the SKA. SISSA, Trieste, PoS(AASKA14)005
Comaschi P., Ferrara A., 2016, MNRAS, preprint (arXiv:1605.06124)
Comaschi P., Ferrara A., 2016, MNRAS, 455, 725
Conroy C., Wechsler R. H., 2009, ApJ, 696, 620
Cooray A., 2016, preprint (arXiv:1602.03512)
Cooray A. et al., 2016, preprint (arXiv:1602.05178)
Crites A. T. et al., 2014, in Holland W. S., Zmuidzinas J., eds, Proc. SPIE Conf. Ser. Vol. 9153, Millimeter, Submillimeter, and Far-Infrared Detectors and Instrumentation for Astronomy. SPIE, Bellingham, p. 91531W
Croft R. A. C. et al., 2015, MNRAS, 457, 3541
Doré O. et al., 2014, preprint (arXiv:1412.4872)
Drake A. B. et al., 2013, MNRAS, 433, 796
Fan X. et al., 2006, AJ, 132, 117
Ferrara A., 2016, in Mesinger A., ed., Astrophysics and Space Science Library, Vol. 423, Understanding the Epoch of Cosmic Reionization. Springer, Berlin, p. 163
Furlanetto S. R., Oh S. P., Briggs F. H., 2006, Phys. Rep., 433, 181
Gong Y., Cooray A., Silva M., Santos M. G., Bock J., Bradford C. M., Zemcov M., 2012, ApJ, 745, 49
Gong Y., Cooray A., Santos M. G., 2013, ApJ, 768, 130
Gong Y., Silva M., Cooray A., Santos M. G., 2014, ApJ, 785, 72
Greve T. R. et al., 2014, ApJ, 794, 142
Gunawardhana M. L. P. et al., 2013, MNRAS, 433, 2764
Helgason K., Ricotti M., Kashlinsky A., 2012, ApJ, 752, 113
Kashlinsky A., 2005, Phys. Rep., 409, 361
Kashlinsky A., Arendt R. G., Mather J., Moseley S. H., 2005, Nature, 438, 45
Leitherer C. et al., 1999, ApJS, 123, 3
Leitherer C., Ekström S., Meynet G., Schaerer D., Agienko K. B., Levesque E. M., 2014, ApJS, 212, 14
Lidz A., Furlanetto S. R., Oh S. P., Aguirre J., Chang T.-C., Doré O., Pritchard J. R., 2011, ApJ, 741, 70
Ly C. et al., 2007, ApJ, 657, 738
McLeod D. J., McLure R. J., Dunlop J. S., 2016, MNRAS, 459, 3812
Matthee J., Sobral D., Santos S., Röttgering H., Darvish B., Mobasher B., 2015, MNRAS, 451, 400
Mo H., van den Bosch F. C., White S., 2010, Galaxy Formation and Evolution. Cambridge Univ. Press, Cambridge
Oesch P. A. et al., 2014, ApJ, 786, 108
Oesch P. A. et al., 2015, ApJ, 804, L30
Ouchi M. et al., 2008, ApJS, 176, 301
Ouchi M. et al., 2010, ApJ, 723, 869
Padmanabhan T., 1993, Structure Formation in the Universe. Cambridge Univ. Press, Cambridge
Planck Collaboration XIII 2015, preprint (arXiv:1502.01589)
Popping G., Pérez-Beaupuits J. P., Spaans M., Trager S. C., Somerville R. S., 2014, MNRAS, 444, 1301
Pullen A. R., Doré O., Bock J., 2014, ApJ, 786, 111
Righi M., Hernández-Monteagudo C., Sunyaev R. A., 2008, A&A, 489, 489
Salvaterra R., Ferrara A., Dayal P., 2011, MNRAS, 414, 847
Schechter P., 1976, ApJ, 203, 297
Silva M. B., Santos M. G., Gong Y., Cooray A., Bock J., 2013, ApJ, 763, 132
Silva M. B., Santos M. G., Cooray A., Gong Y., 2015, ApJ, 806, 209
Silva M., Santos M. G., Cooray A., Gong Y., 2015, ApJ, 806, 209
Vale A., Ostriker J. P., 2004, MNRAS, 353, 189
Vallini L., Gallerani S., Ferrara A., Baek S., 2013, MNRAS, 433, 1567
Vallini L., Gallerani S., Ferrara A., Pallottini A., Yue B., 2015, ApJ, 813, 36
Vázquez G. A., Leitherer C., 2005, ApJ, 621, 695
Visbal E., Loeb A., 2010, J. Cosmol. Astropart. Phys., 11, 16
Visbal E., Trac H., Loeb A., 2011, J. Cosmol. Astropart. Phys., 8, 10
Visbal E., Haiman Z., Bryan G. L., 2015, MNRAS, 450, 2506
Volonteri M., Bellovary J., 2012, Rep. Prog. Phys., 75, 124901
Wang X., Tegmark M., Santos M. G., Knox L., 2006, ApJ, 650, 529
Wolz L. et al., 2015, in Proc. Sci., Foreground Subtraction in Intensity Mapping with the SKA. SISSA, Trieste, PoS(AASKA14)035
Yue B., Ferrara A., Pallottini A., Gallerani S., Vallini L., 2015, MNRAS, 450, 3829

APPENDIX A: PS VARIANCE

In this appendix, we discuss the derivation of the deviate of equation (10). For simplicity, we consider only two components: the line intensity I_α and the detector noise I_N; we will work in $\boldsymbol{k}$-space:

$$\delta I = \delta I_\alpha + \delta I_N. \tag{A1}$$

Since other components do not correlate with I_α and with I_N, adding them to the results is trivial.

In this paper, we use the Fourier convention from Padmanabhan (1993):

$$\delta_k = \int_V \delta(\boldsymbol{x}) e^{-i\boldsymbol{k}\cdot\boldsymbol{x}} d^3\boldsymbol{x}; \tag{A2}$$

δ_k has a Gaussian probability distribution function (PDF). If δ_k is written in polar coordinates, $\delta_k = r_k \exp i\phi_k$, the PDF assumes the form

$$g_k(r_k, \phi_k) \mathrm{d}r_k \mathrm{d}\phi_k = \frac{2r_k \mathrm{d}r_k}{\sigma_k^2} \left(\frac{\mathrm{d}\phi_k}{2\pi}\right) e^{-\frac{r_k^2}{\sigma_k^2}}. \tag{A3}$$

With equation (A3), it is easy to prove that $\langle \delta_k \delta_p^* \rangle = \eta_{kp} \sigma_k^2$ (where η_{kp} is the Kronecker delta function). The cases for δI_α and for δI_N are similar with the only exception that the variance of σ_N does not depend on $\boldsymbol{k}$.

Expanding the first term in equation (9), we get

$$\begin{aligned}
\langle (\delta I \delta I^*)^2 \rangle &= \langle |\delta I_\alpha|^4 \rangle + \langle |\delta_N|^4 \rangle + \langle \delta I_\alpha^2 (\delta I_N^*)^2 \rangle \\
&\quad + \langle (\delta I_\alpha^*)^2 \delta I_N^2 \rangle + 4 \langle |\delta I_\alpha|^2 |\delta I_N|^2 \rangle \\
&\quad + 2 \langle |\delta I_\alpha|^2 \, \delta I_\alpha \delta I_N^* \rangle + 2 \langle |\delta I_\alpha|^2 \, \delta I_\alpha^* \delta I_N \rangle \\
&\quad + 2 \langle \delta I_\alpha \, |\delta I_N|^2 \, \delta I_N^* \rangle + 2 \langle \delta I_\alpha^* \, |\delta I_N|^2 \, \delta I_N \rangle \\
&= \langle |\delta I_\alpha|^4 \rangle + \langle |\delta_N|^4 \rangle + 4 \langle |\delta I_\alpha|^2 |\delta I_N|^2 \rangle,
\end{aligned} \tag{A4}$$

where terms like $\langle (\delta I_\alpha^*)^2 \delta I_N^2 \rangle$ are null because of the averaging over the phase ϕ in equation (A3)

$$\left\langle (\delta I_\alpha^*)^2 \delta I_N^2 \right\rangle \propto \int \mathrm{d}\phi_\alpha \mathrm{d}\phi_N e^{-2i\phi_\alpha} e^{2i\phi_N} = 0. \tag{A5}$$

The second term in equation (9) is

$$\langle (\delta I \delta I^*) \rangle^2 = \left(\langle |\delta I_\alpha|^2 \rangle + \langle |\delta_N|^2 \rangle \right)^2. \tag{A6}$$

Using the fact that both δI_α and δI_N are Gaussian, we have

$$\langle |\delta_k|^4 \rangle = \int r_k^4 \frac{\mathrm{d}r_k^2}{\sigma_k^2} e^{-\frac{r_k^2}{\sigma_k^2}} = 2\sigma_k^4, \tag{A7}$$

and finally

$$\langle (\delta I \delta I^*)^2 \rangle - \langle (\delta I \delta I^*) \rangle^2 = \left(\langle |\delta I_\alpha|^2 \rangle + \langle |\delta_N|^2 \rangle \right)^2. \tag{A8}$$

This paper has been typeset from a TEX/LATEX file prepared by the author.